Nanoscale

Synthesis and formulation of functional bionanomaterials with superoxide dismutase activity†

Marko Pavlovic, Paul Rouster and Istvan Szilagyi*

Layered double hydroxide (LDH) nanoparticles were prepared and used as solid support for superoxide dismutase (SOD) enzymes. Structural features were studied by XRD, spectroscopic methods (IR, UV-Vis and fluorescence) and TEM, while colloidal stability of the obtained materials was investigated by electrophoresis and light scattering in aqueous dispersions. The SOD quantitatively adsorbed on the LDH by electrostatic and hydrophobic interactions and kept its structural integrity upon immobilization. The composite material showed moderate resistance against salt-induced aggregation in dispersions, therefore, heparin polyelectrolyte was used to improve the colloidal stability of the system. Heparin of highly negative line charge density strongly adsorbed on the oppositely charged hybrid particles leading to charge neutralization and overcharging at appropriate polyelectrolyte loading. Full coverage of the composite platelets with heparin resulted in highly stable dispersions, which contained only primary particles even at elevated ionic strengths. Our results indicate that the developed bionanocomposite of considerable enzymatic function is a suitable candidate for applications, wherever stable dispersions of antioxidant activity are required for instance in biomedical treatments or in chemical manufacturing processes.

Introduction

Immobilization of native enzymes attracts widespread contemporary interest as indicated by the considerable number of reviews released recently in this topic in the chemical literature.[1–5] Enzymes attached to solid supports are widely used in catalysis,[6] analytical chemistry,[7] biotechnology,[8] water treatment[9] and in numerous chemical manufacturing processes.[10,11] Several immobilization techniques have been described, where carrier substances included insoluble inorganic particles (*e.g.*, silica,[12] carbon derivatives,[13] iron oxide,[14] metal–organic frameworks,[4] zirconium phosphate,[15] titania[16] and clays[17,18]), polymers[19–21] or hybrid materials.[22] The attachments were carried out by various forces (electrostatic interaction, physical adsorption, covalent linkage, *etc.*). One of the most important conclusions was that the matrix has to provide an environment, which is biocompatible and chemically inert. Consequently, the interaction with the solid support should not change the protein structure responsible for the enzymatic activity, but should be able to defend it from

Department of Inorganic and Analytical Chemistry, University of Geneva, 30 Quai Ernest-Ansermet, CH-1205 Geneva, Switzerland.
E-mail: istvan.szilagyi@unige.ch; Tel: +41223796031
†Electronic supplementary information (ESI) available. See DOI: 10.1039/c6nr07672f

environmental effects, which can lead to denaturation and loss of activity.[23]

Lamellar clay materials possess several advantageous properties, which make them popular solid supports in enzyme immobilization processes usually taking place through electrostatic interactions.[7,24,25] Accordingly, the protein loading is often high due to the significant ion exchange capacity of the clays, the electrostatic attraction provides a strong attachment, the distance between the lamellae can be tuned and pillared materials can be obtained, delamination into unilamellar nanosheets results in dispersions of high surface area and clays are available in large amount in nature or their preparation is relatively uncomplicated.

Among them, layered double hydroxides (LDHs) are one of the most popular enzyme carriers.[7,18,25] LDHs are hydrotalcite-type anionic (*i.e.*, with anion exchange capacity) clays containing lamellar mixed hydroxides with exchangeable anions and water between the layers.[26] Although LDHs are less frequent than the cationic clays in nature, their synthesis is simple even in large amount and various methods are available.[27–32] The structure of the LDHs is based on $Mg(OH)_2$ (brucite) of octahedral coordination around the metal ions. The Mg^{2+} can be substituted with trivalent cations (*e.g.*, Al^{3+} and Fe^{3+}) of similar coordination properties. This isomorphous substitution results in positively charged layers neutralized electrically by anions, which can be exchanged to other negatively

charged substances. The Mg^{2+} can also be replaced by other divalent metal ions (Fe^{2+}, Zn^{2+}, Ca^{2+}, *etc.*) leading to high compositional diversity of the LDH materials.

Amylase enzyme was adsorbed on Mg/Al-CO$_3$-LDH (*i.e.*, composed of Mg^{2+} and Al^{3+} layer forming metal ions and CO_3^{2-} charge compensating anions) resulting in a biohybrid, which showed excellent activity in hydrolyzing starch.[33] LDH-enzyme composites were also prepared for the development of biosensors. For example, Zn/Al-alginate-LDH was used to entrap polyphenol oxidase and the obtained composite material showed high sensitivity in catechol detection.[34] In another system, the conformation of pancreatic lipase upon adsorption on lactate-intercalated LDH was tuned by optimizing the enzyme-to-LDH ratio in the reaction mixture.[35] Urease enzyme was immobilized in/on Zn/Al-Cl-LDH in different ways. Namely, physically adsorbed on the outer surface and intercalated into the interlamellar space by the delamination-restacking method or during the coprecipitation process.[36] The latter method resulted in the highest amount of enzyme in the composite and the developed materials showed sufficient activity in urea hydrolysis. Such a coprecipitation method was also used to intercalate papain in an LDH containing Mg^{2+} and Al^{3+} metal ions in the lamellae.[37] The structure and the activity of the enzyme was the same after de-intercalation from the hybrid material indicating that the solid support is suitable to provide time-controlled release of papain.

Antioxidant enzymes including superoxide dismutase (SOD) are an important class of proteins for therapeutic applications and in various industrial manufacturing processes due to their high efficiency in decomposition of reactive oxygen species (ROS).[38] Immobilization of SOD on suitable solid supports has been performed to improve its formulation, reusability and resistance against the environmental effects (*e.g.*, change in pH, temperature or ionic strength).

Accordingly, SOD was physically adsorbed and covalently grafted to functionalized silica microspheres and the obtained composites showed excellent activity in decomposition of superoxide radicals.[39] Titania nanosheet–SOD hybrid material was found to be more active in enzymatic assays than the native protein.[40] SOD was covalently attached to carbon nanotubes and the highly dispersible composites successfully decreased the oxidative stress caused by ROS in living systems.[41] Other carbon derivatives were also used to immobilize the natural enzyme on electrode surfaces to develop biosensors in order to determine the concentration of superoxide radicals in biological samples.[42,43] Moreover, hydrogel vehicles were synthesized and SOD was encapsulated inside the nanoparticles to get protected from antibodies and degradation.[44] The immobilization process did not affect the catalytic activity and the developed system was proposed as a promising tool for enzymatic therapy.

Besides, to replace the sensitive and hardly manageable native SOD, artificial enzymes composed of transition metal complexes or other inorganic substances of sufficient SOD-like activity were prepared and immobilized in/on silica,[45,46] montmorillonite,[47,48] carbon nanotube[49] and polymer[50] particles.
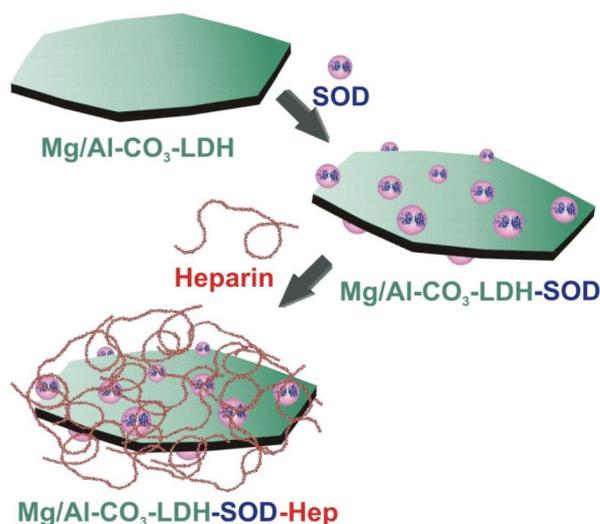
Scheme 1 Schematic representation of the SOD immobilization and heparin coating processes.

In the above examples, the researchers focused on the synthesis, solid state characterization and enzymatic activity tests of the hybrid materials. In spite of the fact that the majority of the applications takes place in heterogeneous systems, mostly in aqueous dispersions, no systematic studies dealing with the colloidal stability of the carrier-enzyme composites have been reported yet. This topic is extremely important, since aggregation of the carrier particles may result in inefficient catalytic activity and failure in enzyme delivery. For instance, immobilization of SOD on suitable solid supports may protect the enzyme during parenteral supplementation into human body, nevertheless, formation of irregularly shaped clusters upon particle aggregation may prevent the successful delivery and may block the veins and cause thrombosis.[51]

In the present study, we aimed at the design of stable dispersions consisting of SOD enzyme immobilized on Mg/Al-CO$_3$-LDH particles. The colloidal stability of the obtained biohybrid was tuned by surface functionalization with heparin polyelectrolyte (Scheme 1). The structure of the composite materials was investigated by microscopic and spectroscopic techniques, while charging and aggregation were probed by electrophoresis and light scattering. The bionanocomposites were applied in enzymatic assays, where they showed excellent superoxide radical scavenging activity. The results shed light on the importance of polyelectrolyte coating in order to obtain highly stable dispersions of antioxidant activity, which are suitable candidates for enzyme-based therapies in living systems for instance.

Experimental

Materials

The chemicals were of high purity level and commercially available substances purchased from Sigma-Aldrich with the

exception of sodium heparin, which was bought from Acros Organics. Enzymes, $Cu^{2+}–Zn^{2+}$ superoxide dismutase from bovine erythrocytes (SOD, EC 1.15.1.1) and xanthine oxidase from bovine milk (EC 1.17.3.2.), were purchased in the form of lyophilized powder, which was dissolved in water for the measurements. Ultrapure water (Millipore) was used for sample preparation and the experiments were carried out at 25.0 ± 0.2 °C and at pH 7.5 ± 0.2, unless otherwise specified. To prepare phosphate buffer, precisely calculated amounts of sodium phosphate dibasic and sodium phosphate monobasic salt solutions were mixed together.

Synthesis of Mg/Al-CO$_3$-LDH

The LDH material (Mg/Al-CO$_3$-LDH) was prepared by the flash coprecipitation method[31,52,53] followed by a hydrothermal treatment in order to improve the particle size distribution.[30] Briefly, 2.564 g of $Mg(NO_3)_2 \cdot 6H_2O$ and 1.876 g of $Al(NO_3)_3 \cdot 9H_2O$ were mixed together and dissolved in 100 mL of water under magnetic agitation. Then 1.060 g of Na_2CO_3 was dissolved in 20 mL of 1 M NaOH solution and added to the previous sample. The obtained solution was stirred for 24 hours and the pH was kept at 9.0 ± 0.5. The solid precipitate was filtered (Nalgene Nylon Membrane Filter of 0.2 μm pore size) and washed extensively with water. After the washing step, the powder was dried overnight in an oven at 60 °C. The synthesized dried powder was dispersed in water to obtain a 4 wt% dispersion. The sample was then transferred in a teflon-lined autoclave (Col-Int Tech), which was sealed and a hydrothermal treatment was performed at 120 °C for 24 hours. After this procedure, the autoclave was removed from the oven and allowed to cool down at ambient temperature. The obtained product was washed several times with water during centrifugation and it was finally dispersed in water to get a 10 wt% stock dispersion and stored in the fridge. Before usage, this stock was diluted and treated in an ultrasonic bath for 5 min.

Synthesis of Mg/Al-CO$_3$-LDH-SOD composite

The composite material consisting of Mg/Al-CO$_3$-LDH and SOD at a dose of 1 mg of SOD per 1 g of particle was prepared as follows. 0.1 mL of Mg/Al-CO$_3$-LDH dispersion at 10 000 mg L^{-1} concentration was mixed with 0.1 mL of SOD solution (10 mg L^{-1}) and 4.8 mL water. The reaction took place during 6 hours to allow the SOD to adsorb on the surface of the LDH particles. Finally, 5 mL of 2 mM phosphate buffer solution was added to set the concentration of the composite material at 100 mg L^{-1} and the total phosphate concentration at 1 mM. This stock dispersion was used for all of the further experiments.

X-ray diffraction

In order to confirm the formation of the Mg/Al-CO$_3$-LDH particles, X-ray diffraction (XRD) measurements were performed on an Empyrean diffractometer (Panalytical) using the CuKα_1 radiation (wavelength of 0.15406 nm). The LDH powder was placed on an 8 mm glass capillary and the data were collected in the 2θ range of 5–65°. The diffractogram of the glass capillary was also recorded and subtracted from the XRD pattern of the material.

Electrophoresis and light scattering

Electrophoretic mobilities were determined with a ZetaNano ZS (Malvern) instrument, while dynamic light scattering (DLS) measurements were performed with a CGS-3 goniometer system (ALV) at a scattering angle of 90°. In the time-resolved DLS experiments, the correlation functions were collected during 10–100 min depending on the speed of particle aggregation. For both experimental techniques, the samples were prepared in a similar manner. Dispersions prepared for electrophoretic mobility measurements were equilibrated overnight, while colloidal stability was probed immediately after sample preparation, in which aqueous solutions of calculated amount of polyelectrolyte and salt were mixed with stable dispersions resulting in 10 mg L^{-1} final particle concentration. The colloidal stability was expressed in terms of stability ratio.[53–55] It should be noted here that stability ratios close to one indicate rapid particle aggregation and unstable systems, while higher values refer to slower aggregation and more stable dispersions.

Spectroscopy

Infrared (IR) spectra were measured in the attenuated total reflectance (ATR) mode with a Spectrum 100 FT-IR spectrometer (PerkinElmer). The ATR crystal was made of diamond. Prior to the IR measurements, the internal reflection unit was washed with ethanol and dried. The solid material was placed on the ATR crystal and the spectrum was recorded in the wavenumber range of 4000 and 400 cm^{-1} at a resolution of 4 cm^{-1}.

UV-Vis absorption spectra were measured at wavelengths between 350 and 800 nm on a Lambda 35 spectrophotometer (PerkinElmer) using glass cuvettes (Hellma) cleaned with a 2 wt% Hellmanex solution (Hellma).

The fluorescence spectra of the bare and immobilized SOD were measured as follows. The enzyme was excited at a wavelength of 283 nm and the emission wavelength was recorded from 293 to 500 nm. A slit of 4 nm and 3 nm was used for the excitation and emission wavelength, respectively. All the spectra were recorded with a Flourolog spectrometer (Horiba Jobin Yvon) using a 450 W xenon lamp.

Microscopy

The morphology of the materials was studied by transmission electron microscopy (TEM) and by scanning electron microscopy (SEM). The TEM images were recorded on a Tecnai G2 Sphera microscope (FEI) at an acceleration voltage of 120 kV using a LaB6 cathode. The samples were prepared by placing 5 μL of solution on the plasma treated carbon mesh and by removing the excess liquid after 2 min. The obtained mesh with the material was installed on the sample holder and placed in the microscope.

For SEM imaging, 20 μL dispersion was deposited on the surface of an adhesive tape previously placed on the sample holder. After the evaporation of the solution, the sample

holder with the remaining material was gold coated. All the SEM images were obtained on a JSM-6510LV microscope (Jeol) with an acceleration voltage of 20 kV.

Determination of the SOD concentration

The SOD content that remained in the solution after the adsorption process was measured by the Bradford test.[56] A stock solution of Coomassie Brilliant Blue dye was prepared by dissolving 100 mg in 50 mL of 95% ethanol and by adding 100 mL of 85% phosphoric acid. The solution was then completed with water to 1000 mL in a volumetric flask. Standard solutions of SOD ranging from 1 mg L^{-1} to 20 mg L^{-1} were prepared and the UV-Vis spectra were recorded after the addition of the dye.

SOD assay

To determine the enzymatic activity of the bare and immobilized SOD, the classical Fridovich method was used.[57] Accordingly, the system contained xanthine and xanthine oxidase to produce superoxide radicals and nitroblue tetrazolium (NBT) as a scavenger indicator. For a typical test reaction, 0.1 mL of 3 mM xanthine, 0.1 mL of 3 mM NBT and 0.3 mL of 3 mg mL^{-1} xanthine oxidase solution were mixed together followed by the addition of 0.1–2.5 mL of the enzyme containing samples. The above listed solutions were all prepared in phosphate buffer at pH 7.5 applying a total phosphate concentration of 1 mM. Upon the reduction of the NBT by the superoxide radicals, it changes its color from yellow to blue and the appearance of an absorption peak at 565 nm was followed with a spectrophotometer (Fig. S1†). Therefore, the absence or only slight formation of the reduced NBT evidences a strong SOD activity, *i.e.*, the efficient capture of the superoxide radicals. The inhibition (I) of the NBT-superoxide radical reaction was calculated by the following equation:

$$I = \frac{\Delta A_S - \Delta A_0}{\Delta A_0} \times 100 \qquad (1)$$

where ΔA_S and ΔA_0 correspond to the increase in absorbance at 565 nm during 5 min, as a consequence of the formation of the reduced form of NBT in the sample with SOD activity and without any SOD activity, respectively. The inhibition is given in percentage and the so-called IC$_{50}$ value represents the concentration of the enzyme corresponding to 50% inhibition.

Results and discussion

The structure of the bare Mg/Al-CO$_3$-LDH was characterized in solid state and its size and charge in aqueous dispersions. SOD adsorption was quantified and the obtained biohybrid was studied by TEM, SEM and by fluorescence and IR spectroscopy. Particle aggregation[53–55,58,59] was followed by DLS, where the colloidal stability as a function of salt and polyelectrolyte concentration was investigated, while electrophoresis was used to probe the charging behavior of the bare and coated particles. These characterizations were performed in two types of media, namely in NaCl solutions and in phosphate buffer to test the ion specific effects on the dispersion properties. The enzymatic function of the obtained hybrid materials was finally tested.

Characterization of Mg/Al-CO$_3$-LDH nanoparticles

The XRD pattern of the synthesized Mg/Al-CO$_3$-LDH was recorded and the peaks were assigned to the respective diffraction planes (Fig. S2†). It was found that all the characteristic bands reported for hydrotalcite-like materials[26] are present indicating the successful synthesis of the lamellar compound. The LDH lattice parameters such as the thickness of the layer with interlayer space (d), the height of the platelets (ν) with the number of sheets assembling in one platelet (n) and the average distance between the metal cations in the sheets (a) were calculated. The ν value was obtained by employing the Scherrer equation[26] and it was found to be 15.92 nm. By dividing the parameter ν with d, the n value was determined and showed that approximately 21 lamellae construct one platelet. Eventually, twice the position of the (110) reflection gave us an average a value of 0.30 nm. Such dimensions are typical for LDH materials.[26,53,60] TEM experiments were performed to characterize the morphology of the Mg/Al-CO$_3$-LDH material (Fig. S3†). Platelets of distorted cylindrical shape were observed in the images.

DLS measurements carried out in stable dispersions yielded a hydrodynamic radius of 110 nm and a polydispersity index of 0.30 indicating a relatively narrow particle size distribution of the Mg/Al-CO$_3$-LDH. The charging and aggregation properties were investigated in NaCl and phosphate buffer solutions (Fig. 1).
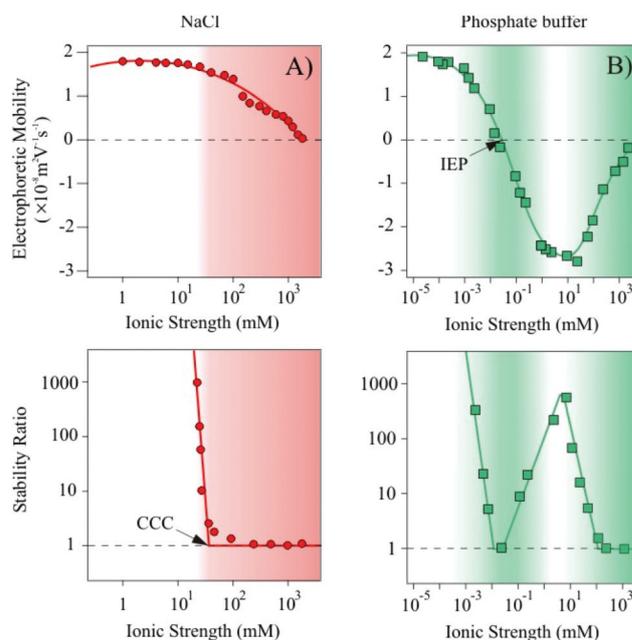

Fig. 1 Top: electrophoretic mobiles of Mg/Al-CO$_3$-LDH particles at different ionic strength set by NaCl (A) or phosphate buffer (B). Bottom: corresponding stability ratio values measured in the same systems. The lines are to guide the eyes and the shaded fields indicate the ionic strength range, where aggregation of the particles takes place.

Let us first discuss the situation, where the ionic strength was set by NaCl (Fig. 1A). At low ionic strength, the measurements yielded positive electrophoretic mobilities. By increasing the salt level, and therefore, the counterion concentration, screening of the particle charge occurred leading to a progressive decrease in the mobility values. The trend in the stability ratios measured under similar experimental conditions shows a decrease (i.e., increasing aggregation rates) with increasing the NaCl concentration, while the values remained close to one at higher ionic strengths. The break point is referred to as the critical coagulation concentration (CCC).[61] Note that stability ratios close to unity indicate rapid (diffusion limited) particle aggregation, while higher values are signals for slow (reaction limited) aggregation processes.

However, when the ionic strength is set by phosphate buffer the situation is more complex (Fig. 1B). At low salt concentrations, the particles exhibit very similar electrophoretic mobilities compared to the ones determined for the NaCl system, nevertheless, the mobilities rapidly decrease by further addition of salt. Charge neutralization occurred at the isoelectric point (IEP) due to the adsorption of the phosphate species on the oppositely charged particles. Moreover, further adsorption resulted in a significant overcharging leading to Mg/Al-CO$_3$-LDH of highly negative charge. An increase in the electrophoretic mobilities was observed at high ionic strength due to the screening effect of the Na$^+$ counterions on the negatively charged surface.

High stability ratios indicated stable dispersions at low phosphate concentrations, while the values decreased with the salt level until reaching the CCC. The CCC value was found to be in the same range of ionic strength as the IEP obtained from the mobility measurements. However, after a narrow instability region, where the stability ratios were found to be equal to unity within the experimental error, the aggregation slowed down and a maximum was observed in the stability ratios. This maximum appeared at similar phosphate concentrations, where the overcharging maximum occurred. Further increase in the phosphate level led to an acceleration of the aggregation and to unstable systems at higher ionic strengths.

Such charging and aggregation behaviors can fairly be explained by the theory of Derjaguin, Landau, Verwey and Overbeek (DLVO).[61] Accordingly, particles of sufficiently high charge possess an electrical double layer around them leading to an interparticle repulsion upon approach towards another particle. This electrical double layer can either be screened away by salts or can vanish due to charge neutralization by counterion adsorption. In the absence of the electrical double layer repulsion, attractive van der Waals forces predominate and hence, the particles rapidly aggregate.

In our systems, destabilization occurred by charge screening in the NaCl samples. For the phosphate buffer, the first fast aggregation regime is clearly owing to the charge neutralization upon phosphate adsorption, while the second destabilization at high concentration is caused by the screening effect of the Na$^+$ ions. In addition, the intermediate restabilization maximum is due to the remarkable overcharging and subsequent re-establishment of the repulsive electrical double

layer forces. Similar trends in the colloidal stability have already been reported for LDH particles in the presence of mono or multivalent anions.[52,60]

Adsorption of SOD on the Mg/Al-CO$_3$-LDH platelets

SOD was adsorbed on the Mg/Al-CO$_3$-LDH platelets. Since the enzyme and the platelets are oppositely charged at the pH used, we have first followed the charging and aggregation behavior of the particles at different SOD doses at 1 mM ionic strength. This allowed us to determine the protein loadings, which do not destabilize the colloidal dispersion of Mg/Al-CO$_3$-LDH. We found that the surface charges were not affected by the SOD adsorption up to an enzyme dose of 10 mg g^{-1} (meaning 10 mg of SOD per 1 g of Mg/Al-CO$_3$-LDH) resulting in stable dispersions under these experimental conditions (Fig. S4†). However, addition of higher amount of enzyme gave rise to charge neutralization and overcharging leading to unstable dispersions near the IEP and to restabilization of the samples at higher loading. The tendency in the aggregation processes can be explained similarly to the case discussed above for the Mg/Al-CO$_3$-LDH platelets in phosphate buffer.

To further prove the adsorption of the enzyme on the surface of the inorganic nanoparticles, the IR spectrum of the Mg/Al-CO$_3$-LDH-SOD composite was measured and compared to the spectra of the native enzyme and bare platelet (Fig. 2). The full assignments of the vibrational bands are shown in Table S1.†

From the IR spectrum of the hybrid material, the characteristic peaks of both the SOD and the Mg/Al-CO$_3$-LDH components could be identified confirming the immobilization of the enzyme on the surface of the particle. Indeed, several peaks corresponding to the inorganic platelets were found in the range of 450–1400 cm^{-1}, in addition to the two absorption bands referring to the bending mode of the CONH amide bond and to the C=C stretching vibration at 1522 cm^{-1} and 1633 cm^{-1}, respect-
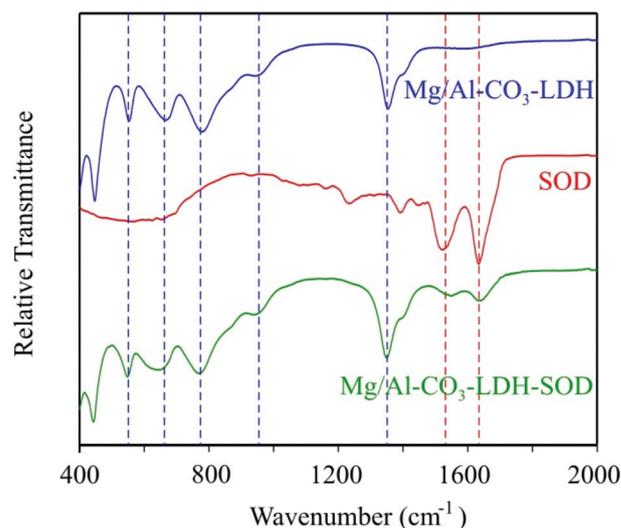

Fig. 2 IR spectra of bare Mg/Al-CO$_3$-LDH, native SOD and the hybrid Mg/Al-CO$_3$-LDH-SOD materials.

ively, of the enzyme.[62] This implies that the adsorption of the SOD did occur on the Mg/Al-CO$_3$-LDH platelets resulting in the formation of the desired composite material.

Besides, the XRD pattern of the Mg/Al-CO$_3$-LDH-SOD was recorded (Fig. S2†). The position of the (003) peak remained unchanged upon addition of SOD indicating no enzyme intercalation between the layers, but rather adsorption on the outer surface. Potential intercalation would increase the interlayer spacing and it would lead to a shift in the location of the (003) diffraction plane.[26]

The adsorption process was also quantified using the Bradford method to determine the SOD concentration in the solutions.[56] In this experiment, 0.1 mL of 10 000 mg L^{-1} of particles and 0.1 mL of 100 mg L^{-1} of enzyme (corresponding to a SOD dose of 10 mg g^{-1}) were mixed together and diluted with 0.3 mL water. The solid material was then filtered off and the Bradford reagent was added to the filtrate. The UV-Vis absorption spectrum was recorded thereafter. The obtained results together with three reference measurements containing different amount of native SOD are shown in Fig. 3.

The absorbance decreases at 465 nm and increases at 595 nm by increasing the enzyme concentration. These shifts of the absorption maximum are based on the binding of the dye to the SOD. The UV-Vis spectrum of the filtrate was identical to the one of the reference sample, which contained no SOD molecules. This finding clearly shows that the enzyme quantitatively adsorbed on the Mg/Al-CO$_3$-LDH and that no partitioning between the bulk and surface took place. We assume that the strong attractive forces between the enzyme and the solid support were achieved through electrostatic and hydrophobic interactions as well as by hydrogen bonding. Similarly high affinity has already been reported earlier for polyelectrolytes adsorbing on oppositely charged surfaces.[53,55,60,63,64] It should also be noted that these results
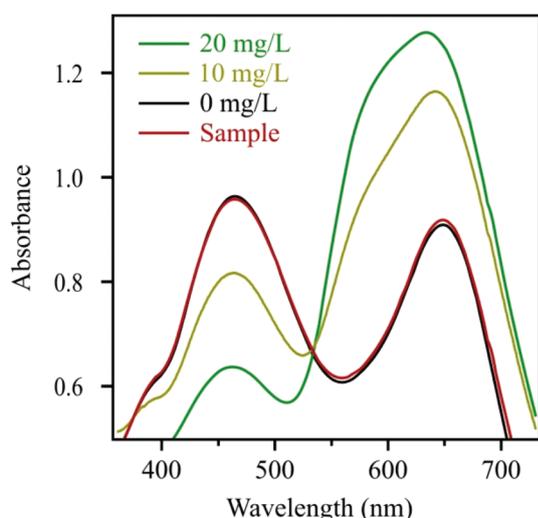
indicate quantitative adsorption at SOD doses lower than 10 mg g^{-1} too.

Polyelectrolyte coating

Although SOD was successfully immobilized on the Mg/Al-CO$_3$-LDH without significantly changing the colloidal stability of the dispersions, this stability is limited and the particles already aggregated at moderate ionic strengths, as discussed earlier. In order to improve their resistance against salt-induced aggregation, the Mg/Al-CO$_3$-LDH-SOD was coated with heparin, which is a biocompatible anticoagulant possessing one of the highest negative line charge density within the natural polyelectrolytes.[65,66] Its effect on colloidal stability of LDH platelets has already been reported.[53]

First, the charging and the aggregation processes in the Mg/Al-CO$_3$-LDH-SOD dispersions were investigated by electrophoresis and DLS, respectively. The measurements were carried out at different heparin doses to probe the effect of its adsorption on the colloidal stability and to determine the experimental conditions where highly stable dispersions can be obtained. The recorded electrophoretic mobilities and stability ratios are shown in Fig. 4.
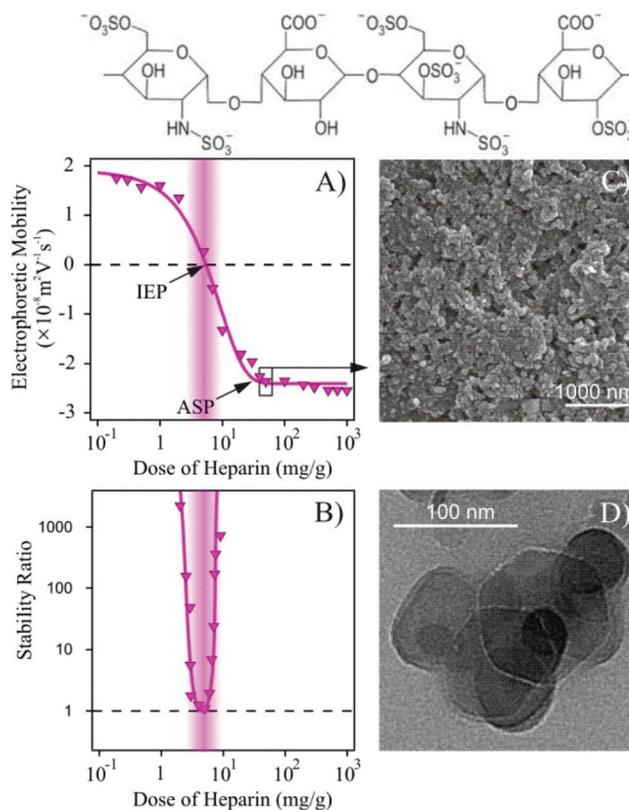

Fig. 4 Electrophoretic mobilities (A) and stability ratios (B) of Mg/Al-CO$_3$-LDH-SOD (1 mg g^{-1} enzyme load) as a function of the heparin concentration. The measurements were performed at 1 mM NaCl and at 10 mg L^{-1} particle concentration. SEM (C) and TEM (D) images of Mg/Al-CO$_3$-LDH-SOD obtained with a 50 mg g^{-1} heparin coverage. The dose of heparin indicates mg of polyelectrolyte per 1 g of particle. The schematic representation of the heparin structure is shown on the top.

Fig. 3 Bradford tests for standard solutions of SOD of 10 mg L^{-1} and 20 mg L^{-1} concentrations and for the reference system without enzyme (0 mg L^{-1}) as well as for the filtrate after the SOD adsorption process (sample).

Increasing the dose of heparin initially led to a decrease in the mobilities, which reached the IEP due to the adsorption of the polyelectrolyte on the oppositely charged platelets (Fig. 4A). Further addition of heparin gave rise to overcharging and the mobilities decreased until the appearance of an adsorption saturation plateau (ASP). The onset of the ASP (around 20 mg g^{-1}) corresponds to the highest possible dose of heparin that can be adsorbed on the particle surface leading to fully coated platelets (Mg/Al-CO$_3$-LDH-SOD-Hep). Above this value, no more heparin adsorption is possible on the particles. These phenomena have already been reported in similar LDH-heparin systems[53] and also for other polyelectrolytes in the presence of oppositely charged particles.[58,63,64]

The stability ratios show an extremely narrow curve (Fig. 4B). The particles are unstable around the IEP due to the lack of stabilizing electrical double layers. The partially coated Mg/Al-CO$_3$-LDH-SOD of positive charge as well as the negatively charged fully coated ones form stable dispersions at this low ionic strength. As predicted by the DLVO theory, the aggregation is hindered by the repulsive electrical double layer forces, whenever the particles possess sufficiently high surface charge.

The hydrodynamic radii of the Mg/Al-CO$_3$-LDH, Mg/Al-CO$_3$-LDH-SOD and Mg/Al-CO$_3$-LDH-SOD-Hep particles were determined in stable dispersions at 1 mM ionic strength and they were found to be 110 nm, 106 nm and 111 nm, respectively. These values are within the experimental error of the DLS method (±5 nm) and hence, one can realize that the SOD adsorption and heparin coating did not change the hydrodynamic radius of the bare Mg/Al-CO$_3$-LDH significantly. This finding is in good agreement with hydrodynamic layer thickness data of polyelectrolyte chains adsorbed on colloidal particles.[67] Accordingly, thicknesses of up to 3 nm were reported at low ionic strengths and hence, considerable increase in the size of the Mg/Al-CO$_3$-LDH platelets cannot be expected upon adsorption of SOD and heparin.

XRD pattern of the Mg/Al-CO$_3$-LDH-SOD-Hep composite was measured to check the possible intercalation of the polyelectrolyte between the lamellae (Fig. S2†). The location of the characteristic (003) peak, which is related to the interlayer distance,[26] did not change significantly upon addition of the polyelectrolyte. This fact indicates that heparin intercalation did not take place and that it adsorbed on the outer surface of the particles. Similar observation was reported with other LDH platelets in the presence of heparin.[53]

The IR spectrum of the Mg/Al-CO$_3$-LDH-SOD-Hep material was found to be very similar to the one measured for the Mg/Al-CO$_3$-LDH-SOD (Fig. S5†) indicating that such a low amount of heparin cannot be detected by this technique.

Fig. 4C and D show the SEM and TEM images, respectively, at doses, where the Mg/Al-CO$_3$-LDH-SOD platelets are fully coated with heparin. The TEM image confirms the above mentioned stability. Accordingly, primary particles can be observed on the picture indicating stable dispersions of the Mg/Al-CO$_3$-LDH-SOD-Hep composites. Their shape was found to be very similar to the ones observed for the bare Mg/Al-CO$_3$-LDH plate-
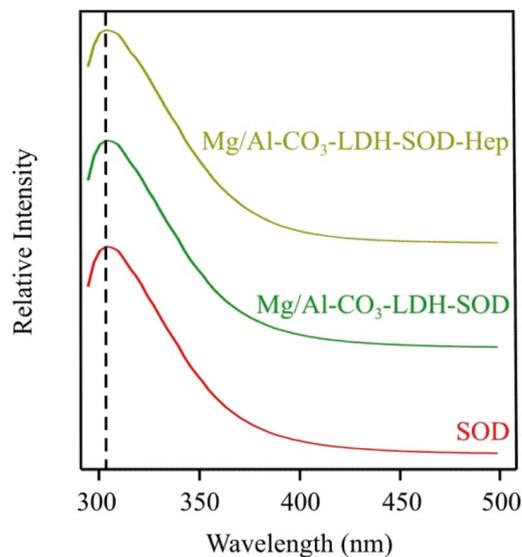

Fig. 5 Emission fluorescence spectra of SOD, Mg/Al-CO$_3$-LDH-SOD and Mg/Al-CO$_3$-LDH-SOD-Hep. The dashed line indicates the intensities at 306 nm wavelength.

lets (Fig. S3†). It should also be noted that the presence of a few aggregates may originate from the drying process during the sample preparation. Additionally, it was observed from the SEM image that the morphology of the material did not undergo any significant changes upon the SOD doping or heparin coating and exhibits typical LDH-type structure.

Fluorescence spectroscopy has been applied to probe the possible conformational changes in the SOD structure that can occur upon its adsorption on the Mg/Al-CO$_3$-LDH surface and during the coating procedure with heparin (Fig. 5).

The 4-hydroxyphenyl side chain groups of the two tyrosine amino acids present in the protein were excited at a wavelength of 283 nm and the fluorescence intensities were followed in the emission wavelength range of 293–500 nm. The intensities at 306 nm wavelength and the recorded emission spectra were found to be similar for all the materials. This finding indicated that the microenvironment of the tyrosine side chains did not change upon their adsorption or coating. This information is crucial, because it indicates that the structural integrity of the SOD enzyme appears preserved meaning that it should lead to similar enzymatic activity in its bare, immobilized and coated forms. This issue will be further discussed later.

Resistance against salt induced aggregation

In the previous sections, we have found that the dispersions of both Mg/Al-CO$_3$-LDH-SOD and Mg/Al-CO$_3$-LDH-SOD-Hep particles were stable at 1 mM ionic strength. However, the ionic strength is usually much higher in bioapplications, e.g., 160 mM in blood.[68] Therefore, we have further investigated the charging and aggregation of the bare and heparin-coated hybrid materials of immobilized SOD in a wide range of ionic strengths set either by NaCl or phosphate buffer solutions.
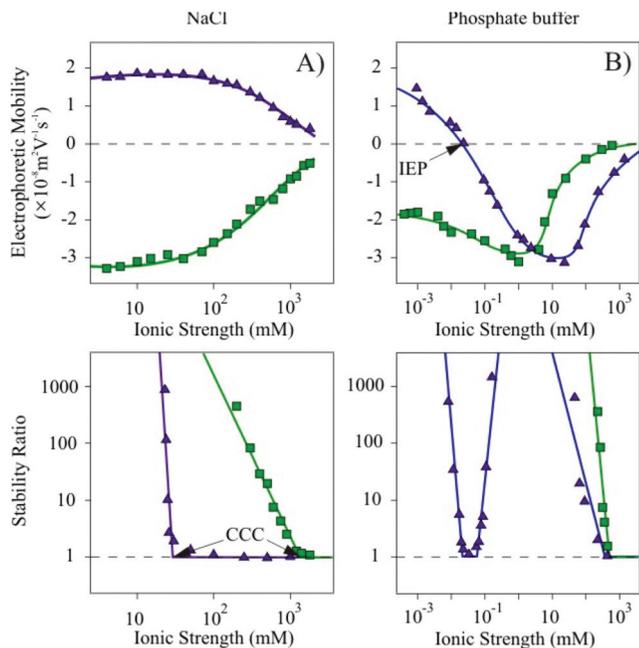
Paper

Nanoscale

Fig. 6 Electrophoretic mobilites (top) and stability ratios (bottom) of Mg/Al-CO₃-LDH-SOD (triangles) and Mg/Al-CO₃-LDH-SOD-Hep (squares) in NaCl (A) and phosphate buffer (B) solutions at different ionic strengths.

In the NaCl series (Fig. 6A), the Mg/Al-CO$_3$-LDH-SOD particles are positively charged, while the Mg/Al-CO$_3$-LDH-SOD-Hep ones are negative in the entire ionic strength range due to the overcharging phenomenon induced by the heparin adsorption, as discussed earlier. By comparing the magnitude of the mobility values at low ionic strengths, it is observed that the heparin-coated particles exhibit a higher surface charge, compared to both the bare and SOD modified nanoplatelets (Fig. 1 and 6A). By increasing the NaCl concentration, the surface charges of the Mg/Al-CO$_3$-LDH-SOD and the Mg/Al-CO$_3$-LDH-SOD-Hep particles are progressively screened by the counterions resulting in a decrease in the magnitude of the electrophoretic mobilities.

In addition, an enormous difference was observed in the CCC values, which were found to be equal to 29 mM and 989 mM for Mg/Al-CO$_3$-LDH-SOD and Mg/Al-CO$_3$-LDH-SOD-Hep, respectively. This 34 times increase induced by the polyelectrolyte coating probably originates from the establishment of two types of repulsive forces. Accordingly, electrical double layer forces are stronger for the Mg/Al-CO$_3$-LDH-SOD-Hep due to their higher surface charge density compared to the bare platelets. Moreover, the adsorbed heparin molecules change their conformation especially at high ionic strengths[67] and hence, polyelectrolyte tails and loops form on the surface leading to steric repulsion between the molecules on the surface, once two coated particles approach each other. Such a powerful electro-steric repulsion has been reported in several polyelectrolyte–particle systems.[53,60,69]

To probe the specific effect of the ionic environment, similar set of experiments was carried out using phosphate buffer instead of NaCl to set the ionic strength. Indeed, significant variations in the charging and aggregation behavior of the particles could be observed by changing the type of anions in the salts (Fig. 6B).

The tendency in the electrophoretic mobilities of the Mg/Al-CO$_3$-LDH-SOD was found to be similar to the one of the Mg/Al-CO$_3$-LDH particles shown in Fig. 1B. Accordingly, the charge neutralization at the IEP as well as the overcharging of Mg/Al-CO$_3$-LDH-SOD occurred by varying the total phosphate concentration.

The colloidal stability was also analogous to the bare nanoplatelets. The stability ratios were high at low salt levels and in the intermediate phosphate concentration regime, while unstable dispersions were observed near the IEP at 0.035 mM and above 500 mM ionic strength due to the vanishing of the electrical double layer forces. The difference between the tendencies in the stability ratios of the Mg/Al-CO$_3$-LDH-SOD particles dispersed in Cl$^-$ or in phosphate medium is striking due to the significant ion specific effects (*i.e.*, due to the dissimilar affinity of these anions to the oppositely charged surface) on the charging and on the corresponding aggregation behavior. In good agreement with our previous study,[52] our present results clearly show that HPO$_4^{2-}$ or H$_2$PO$_4^-$ counterions adsorb strongly, while Cl$^-$ behaves as an indifferent ion and mainly remains in the bulk.

For the polyelectrolyte-coated Mg/Al-CO$_3$-LDH-SOD-Hep, the mobilities follow different tendencies in phosphate buffer. At lower ionic strengths, the materials have high negative surface charge (Fig. 6B). The mobilities show a minimum at 1 mM likely owing to the additional phosphate adsorption on the heparin-coated platelets. The increased Na$^+$ concentration led to charge screening and to an increase in the electrophoretic mobilites at high ionic strengths, but the values remained negative in the entire concentration range investigated.

The dispersions were highly stable until elevated phosphate concentrations due to the above mentioned electro-steric stabilization mechanism and the CCC was located at a very high ionic strength (Fig. 6B). The fact that we found extremely high CCCs for the Mg/Al-CO$_3$-LDH-SOD-Hep platelets in both NaCl and phosphate buffer indicates that the destabilization occurs mainly by the screening effect of the Na$^+$ ions, which are the bulk-forming counterions of the negatively charged particles, and the type of coions (*i.e.*, Cl$^-$, HPO$_4^{2-}$ or H$_2$PO$_4^-$) has no or little influence on the colloidal stability.

Therefore, the advantage of the polyelectrolyte coating is clear. The bare particles aggregate at low ionic strengths in both NaCl and phosphate buffer solutions, whereas the Mg/Al-CO$_3$-LDH-SOD-Hep ones form stable dispersions up to high salt levels. Thus, the latter ones are recommended for biomedical or other industrial applications, where the immobilized enzymes can be dispersed in a mixture of different salts at higher ionic strengths.

Enzymatic function

Although we have designed highly stable Mg/Al-CO$_3$-LDH-SOD-Hep dispersions in the previous section, their ability to

capture superoxide radicals has to be verified in order to use them as antioxidants in any future applications. The enzymatic activity of the hybrid materials was determined by the Fridovich method[57] and compared to the one of native SOD. This assay is based on superoxide radical production from the xanthine–xanthine oxidase system and the inhibition of NBT reduction by the radicals is followed by measuring the color change in the solutions. The activities were quantified with the IC_{50} values, which are the SOD concentrations necessary for the decomposition of half of the superoxide radicals forming in the test reaction.[47,48,50]

Prior to the enzymatic activity measurements with the SOD and its immobilized forms, we have tested the influence of the carrier particles and the coating agent on the probe reaction. The $Mg/Al-CO_3$-LDH did not show any superoxide radical capturing ability in the particle concentration range used in our experiments. The role of the heparin in the assay is especially important to probe, since it can inhibit the xanthine–xanthine oxidase reaction by binding to the xanthine oxidase enzyme, which would lead to a smaller amount of superoxide radicals forming in the solution and to a false IC_{50} value.[70] However, we found that inhibition of the xanthine oxidase takes place only at heparin concentrations above 20 mg L^{-1} (Fig. S6†), which is higher than the maximum polyelectrolyte loading (5 mg L^{-1}) applied in our experiments. Therefore, the heparin content in the $Mg/Al-CO_3$-LDH-SOD-Hep does not affect the superoxide production in the assay.

Moreover, we found that the immobilization and the heparin coating did not change the activity of the SOD enzyme significantly. Very similar IC_{50} values were determined (IC_{50}(SOD) = 0.069 mg L^{-1}; IC_{50}($Mg/Al-CO_3$-LDH-SOD) = 0.056 mg L^{-1} and IC_{50}($Mg/Al-CO_3$-LDH-SOD-Hep) = 0.096 mg L^{-1}) indicating an excellent superoxide radical scavenging activity for all materials. However, the shape of the inhibition versus SOD concentration curve is somewhat different for the $Mg/Al-CO_3$-LDH-SOD material (Fig. S7†). We believe that this deviation originates from the fact that the $Mg/Al-CO_3$-LDH-SOD composite is positively charged and thus, the negatively charged superoxide radicals are attracted electrostatically. This interaction may change the entire dismutation mechanism giving rise to differently shaped inhibition curves.

The fact that the IC_{50} value determined for the $Mg/Al-CO_3$-LDH-SOD-Hep platelets is similar to the one for the native enzyme means that we have successfully developed a colloidal system containing homogeneously dispersed hybrid particles of significant SOD activity. This novel bionanocomposite holds enormous promises for future biomedical applications and industrial manufacturing processes, wherever stable dispersions are required to decompose ROS including superoxide radicals.

Conclusions

We report here on the immobilization of SOD enzyme on a nanoparticulate support and the formulation of the hybrid materials. $Mg/Al-CO_3$-LDH were synthesized by the coprecipitation method and successfully modified with the protein owing to its strong affinity to the surface through electrostatic, hydrophobic and hydrogen bonding interactions. No evidence was found for intercalation of SOD in the interlayer space indicating that the adsorption took place on the outer surface of the particles. The $Mg/Al-CO_3$-LDH-SOD platelets showed moderate colloidal stability, which were sensitive to the ionic environment in the dispersions. Therefore, the resistance against salt-induced aggregation was improved by surface functionalization with heparin. Its adsorption led to charge neutralization and to overcharging at appropriate polyelectrolyte loadings. The presence of the saturated heparin layer on the particle surface resulted in an enormous stabilization effect for the $Mg/Al-CO_3$-LDH-SOD-Hep materials in aqueous dispersions, which were stable up to high ionic strength irrespectively of the type of salt dissolved in the samples. The immobilization did not change the structure of the enzyme and very similar enzymatic activities were determined for the native SOD, $Mg/Al-CO_3$-LDH-SOD and $Mg/Al-CO_3$-LDH-SOD-Hep. To summarize, highly stable dispersions of excellent superoxide radical scavenging activity were developed during the present work. Such systems possess huge potential in applications demanding bionanocatalysts of antioxidant activity used in heterogeneous samples.

Acknowledgements

References

1 R. A. Sheldon and S. van Pelt, Chem. Soc. Rev., 2013, 42, 6223–6235.

2 Y. H. Lin, Z. W. Chen and X. Y. Liu, Trends Biotechnol., 2016, 34, 303–315.

3 V. E. Bosio, G. A. Islan, Y. N. Martinez, N. Duran and G. R. Castro, Crit. Rev. Biotechnol., 2016, 36, 447–464.

4 J. Mehta, N. Bhardwaj, S. K. Bhardwaj, K. H. Kim and A. Deep, Coord. Chem. Rev., 2016, 322, 30–40.

5 A. Popat, S. B. Hartono, F. Stahr, J. Liu, S. Z. Qiao and G. Q. Lu, Nanoscale, 2011, 3, 2801–2818.

6 M. Pita, D. M. Mate, D. Gonzalez-Perez, S. Shleev, V. M. Fernandez, M. Alcalde and A. L. De Lacey, J. Am. Chem. Soc., 2014, 136, 5892–5895.

7 C. Mousty and V. Prevot, Anal. Bioanal. Chem., 2013, 405, 3513–3523.

8 A. Idris and A. Bukhari, Biotechnol. Adv., 2012, 30, 550–563.

9 N. Loncar and Z. Vujcic, *J. Hazard. Mater.*, 2011, **196**, 73–78.

10 A. Liese and L. Hilterhaus, *Chem. Soc. Rev.*, 2013, **42**, 6236–6249.

11 R. DiCosimo, J. McAuliffe, A. J. Poulose and G. Bohlmann, *Chem. Soc. Rev.*, 2013, **42**, 6437–6474.

12 P. Santos-Moriano, L. Monsalve-Ledesma, M. Ortega-Munoz, L. Fernandez-Arrojo, A. O. Ballesteros, F. Santoyo-Gonzalez and F. J. Plou, *RSC Adv.*, 2016, **6**, 64175–64181.

13 J. H. Bartha-Vari, M. I. Tosa, F. D. Irimie, D. Weiser, Z. Boros, B. G. Vertessy, C. Paizs and L. Poppe, *ChemCatChem*, 2015, **7**, 1122–1128.

14 A. Salic, K. Pindric, G. H. Podrepsek, M. Leitgeb and B. Zelic, *Green Process. Synth.*, 2013, **2**, 569–578.

15 I. K. Deshapriya, C. S. Kim, M. J. Novak and C. V. Kumar, *ACS Appl. Mater. Interfaces*, 2014, **6**, 9643–9653.

16 H. Wu, C. H. Zhang, Y. P. Liang, J. F. Shi, X. L. Wang and Z. Y. Jiang, *J. Mol. Catal. B: Enzym.*, 2013, **92**, 44–50.

17 U. Andjelkovic, A. Milutinovic-Nikolic, N. Jovic-Jovicic, P. Bankovic, T. Bajt, Z. Mojovic, Z. Vujcic and D. Jovanovic, *Food Chem.*, 2015, **168**, 262–269.

18 E. Geraud, V. Prevot, C. Forano and C. Mousty, *Chem. Commun.*, 2008, 1554–1556.

19 A. Cerdobbel, T. Desmet, K. De Winter, J. Maertens and W. Soetaert, *J. Biotechnol.*, 2010, **150**, 125–130.

20 A. Fishman, I. Levy, U. Cogan and O. Shoseyov, *J. Mol. Catal. B: Enzym.*, 2002, **18**, 121–131.

21 D. Alsafadi and F. Paradisi, *Mol. Biotechnol.*, 2014, **56**, 240–247.

22 O. Kudina, A. Zakharchenko, O. Trotsenko, A. Tokarev, L. Ionov, G. Stoychev, N. Puretskiy, S. W. Pryor, A. Voronov and S. Minko, *Angew. Chem., Int. Ed.*, 2014, **53**, 483–487.

23 R. C. Rodrigues, C. Ortiz, A. Berenguer-Murcia, R. Torres and R. Fernandez-Lafuente, *Chem. Soc. Rev.*, 2013, **42**, 6290–6307.

24 A. J. Patil and S. Mann, *J. Mater. Chem.*, 2008, **18**, 4605–4615.

25 C. Mousty, *Appl. Clay Sci.*, 2004, **27**, 159–177.

26 D. G. Evans and R. C. T. Slade, in *Layered Double Hydroxides*, ed. X. Duanand D. G. Evans, 2006, vol. 119, pp. 1–87.

27 Q. Wang, S. V. Y. Tang, E. Lester and D. O'Hare, *Nanoscale*, 2013, **5**, 114–117.

28 Z. Ferencz, A. Kukovecz, Z. Konya, P. Sipos and I. Palinko, *Appl. Clay Sci.*, 2015, **112**, 94–99.

29 I. Dekany, F. Berger, K. Imrik and G. Lagaly, *Colloid Polym. Sci.*, 1997, **275**, 681–688.

30 Z. P. Xu, G. Stevenson, C. Q. Lu and G. Q. Lu, *J. Phys. Chem. B*, 2006, **110**, 16923–16929.

31 J. He, M. Wei, B. Li, Y. Kang, D. G. Evans and X. Duan, in *Layered Double Hydroxides*, ed. X. Duanand D. G. Evans, 2006, vol. 119, pp. 89–119.

32 H. F. Bao, J. P. Yang, Y. Huang, Z. P. Xu, N. Hao, Z. X. Wu, G. Q. Lu and D. Y. Zhao, *Nanoscale*, 2011, **3**, 4069–4073.

33 F. Bruna, M. G. Pereira, M. Polizeli and J. B. Valim, *ACS Appl. Mater. Interfaces*, 2015, **7**, 18832–18842.

34 M. S. P. Lopez, F. Leroux and C. Mousty, *Sens. Actuators, B*, 2010, **150**, 36–42.

35 Z. An, S. Lu, J. He and Y. Wang, *Langmuir*, 2009, **25**, 10704–10710.

36 S. Vial, V. Prevot, F. Leroux and C. Forano, *Microporous Mesoporous Mater.*, 2008, **107**, 190–201.

37 N. Zou and J. Plank, *J. Phys. Chem. Solids*, 2012, **73**, 1127–1130.

38 A. Bafana, S. Dutt, S. Kumar and P. S. Ahuja, *Crit. Rev. Biotechnol.*, 2011, **31**, 65–76.

39 Y. M. Fan, X. D. Cao, T. Hu, X. G. Lin, H. Dong and X. N. Zou, *J. Phys. Chem. C*, 2016, **120**, 3955–3963.

40 K. Kamada, A. Yamada and N. Soh, *RSC Adv.*, 2015, **5**, 85511–85516.

41 S. Singh and V. K. Dubey, *Int. J. Pept. Res. Ther.*, 2016, **22**, 171–177.

42 J. Tang, X. Zhu, X. H. Niu, T. T. Liu, H. L. Zhao and M. B. Lan, *Talanta*, 2015, **137**, 18–24.

43 X. Zhu, X. H. Niu, H. L. Zhao, J. Tang and M. B. Lan, *Biosens. Bioelectron.*, 2015, **67**, 79–85.

44 S. Bobone, E. Miele, B. Cerroni, D. Roversi, A. Bocedi, E. Nicolai, A. Di Venere, E. Placidi, G. Ricci, N. Rosato and L. Stella, *Langmuir*, 2015, **31**, 7572–7580.

45 Y. C. Fang, H. C. Lin, I. J. Hsu, T. S. Lin and C. Y. Mou, *J. Phys. Chem. C*, 2011, **115**, 20639–20652.

46 Z. Csendes, C. Dudas, G. Varga, E. G. Bajnoczi, S. E. Canton, P. Sipos and I. Palinko, *J. Mol. Struct.*, 2013, **1044**, 39–45.

47 I. Szilagyi, I. Labadi, K. Hernadi, I. Palinko, I. Fekete, L. Korecz, A. Rockenbauer and T. Kiss, *New J. Chem.*, 2005, **29**, 740–745.

48 I. Szilagyi, I. Labadi, K. Hernadi, T. Kiss and I. Palinko, in *Molecular Sieves: From Basic Research to Industrial Applications, Pts a and B*, ed. J. Cejka, N. Zilkova and P. Nachtigall, 2005, vol. 158, pp. 1011–1018.

49 L. Yuan, S. L. Liu, W. W. Tu, Z. S. Zhang, J. C. Bao and Z. H. Dai, *Anal. Chem.*, 2014, **86**, 4783–4790.

50 I. Szilagyi, O. Berkesi, M. Sipiczki, L. Korecz, A. Rockenbauer and I. Palinko, *Catal. Lett.*, 2009, **127**, 239–247.

51 T. L. Moore, L. Rodriguez-Lorenzo, V. Hirsch, S. Balog, D. Urban, C. Jud, B. Rothen-Rutishauser, M. Lattuada and A. Petri-Fink, *Chem. Soc. Rev.*, 2015, **44**, 6287–6305.

52 M. Pavlovic, R. Huber, M. Adok-Sipiczki, C. Nardin and I. Szilagyi, *Soft Matter*, 2016, **12**, 4024–4033.

53 M. Pavlovic, L. Li, F. Dits, Z. Gu, M. Adok-Sipiczki and I. Szilagyi, *RSC Adv.*, 2016, **6**, 16159–16167.

54 M. Schudel, S. H. Behrens, H. Holthoff, R. Kretzschmar and M. Borkovec, *J. Colloid Interface Sci.*, 1997, **196**, 241–253.

55 K. L. Chen, S. E. Mylon and M. Elimelech, *Langmuir*, 2007, **23**, 5920–5928.

56 M. M. Bradford, *Anal. Biochem.*, 1976, **72**, 248–254.

57 C. Beaucham and I. Fridovich, *Anal. Biochem.*, 1971, **44**, 276–287.

58 A. Tiraferri and M. Borkovec, *Sci. Total Environ.*, 2015, **535**, 131–140.

59 J. Smith, G. B. Webber, G. G. Warr and R. Atkin, *Langmuir*, 2014, **40**, 1506–1513.

60 M. Pavlovic, P. Rouster, T. Oncsik and I. Szilagyi, *ChemPlusChem*, 2016, DOI: 10.1002/cplu.201600295.

61 D. F. Evans and H. Wennerstrom, *The Colloidal Domain*, John Wiley, New York, 1999.

62 J. T. Kloprogge and R. L. Frost, *Appl. Catal., A*, 1999, **184**, 61–71.

63 I. Popa, G. Gillies, G. Papastavrou and M. Borkovec, *J. Phys. Chem. B*, 2010, **114**, 3170–3177.

64 I. Szilagyi, G. Trefalt, A. Tiraferri, P. Maroni and M. Borkovec, *Soft Matter*, 2014, **10**, 2479–2502.

65 G. A. Crespo, M. G. Afshar and E. Bakker, *Angew. Chem., Int. Ed.*, 2012, **51**, 12575–12578.

66 B. Casu, A. Naggi and G. Torri, *Carbohydr. Res.*, 2015, **403**, 60–68.

67 E. Seyrek, J. Hierrezuelo, A. Sadeghpour, I. Szilagyi and M. Borkovec, *Phys. Chem. Chem. Phys.*, 2011, **13**, 12716–12719.

68 I. Bertini, H. B. Gray, S. J. Lippard and J. S. Valentine, *Bioinorganic chemistry*, University Science Books, Mill Valley, 1994.

69 E. Illes and E. Tombacz, *J. Colloid Interface Sci.*, 2006, **295**, 115–123.

70 R. Radi, H. Rubbo, K. Bush and B. A. Freeman, *Arch. Biochem. Biophys.*, 1997, **339**, 125–135.